Advances in Atmospheric Sciences
Impact Factor: 3.158
E-alert
ISSN 0256-1530
CN 11-1925/O4

Response of Freezing/Thawing Indexes to the Wetting Trend under Warming Climate Conditions over the Qinghai Tibetan Plateau during 19612010: A Numerical Simulation

Xuewei FANG, Zhi LI, Chen CHENG, Klaus FRAEDRICH, Anqi WANG, Yihui CHEN, Yige XU, Shihua LYU

Citation: Fang, X. W., Z. Li, C. Cheng, K. Fraedrich, A. Q. Wang, Y. H. Chen, Y. G. Xu, and S. H. Lyu 2023: Response of Freezing/Thawing Indexes to the Wetting Trend under Warming Climate Conditions over the Qinghai Tibetan Plateau during 19612010: A Numerical Simulation, *Adv. Atmos. Sci.*, 40, 211–222. doi: 10.1007/s00376–022–2109–z.

View online: https://doi.org/10.1007/s00376–022–2109–z

ADVANCES IN ATMOSPHERIC SCIENCES, VOL. 40, FEBRUARY 2023, 211–222

• **Original Paper** •

Response of Freezing/Thawing Indexes to the Wetting Trend under Warming Climate Conditions over the Qinghai –Tibetan Plateau during 1961–2010: A Numerical Simulation

Xuewei FANG*[1], Zhi LI[1], Chen CHENG[2], Klaus FRAEDRICH[3], Anqi WANG[1], Yihui CHEN[1], Yige XU[1], and Shihua LYU[1,4]

[1]*Plateau Atmosphere and Environment Key Laboratory of Sichuan Province*, *School of Atmospheric Sciences*, *Chengdu University of Information Technology*, *Chengdu* 610225, *China*

[2]*Southwest Institute of Technical Physics*, *Chengdu* 610225, *China*

[3]*Max Planck Institute for Meteorology*, *Hamburg* 20146, *Germany*

[4]*Collaborative Innovation Center on Forecast and Evaluation of Meteorological Disasters*, *Nanjing University of Information Science & Technology*, *Nanjing* 210044, *China*

(Received 7 May 2022; revised 21 July 2022; accepted 15 August 2022)

ABSTRACT

Since the 1990s, the Qinghai–Tibetan Plateau (QTP) has experienced a strikingly warming and wetter climate that alters the thermal and hydrological properties of frozen ground. A positive correlation between the warming and thermal degradation in permafrost or seasonally frozen ground (SFG) has long been recognized. Still, a predictive relationship between historical wetting under warming climate conditions and frozen ground has not yet been well demonstrated, despite the expectation that it will become even more important because precipitation over the QTP has been projected to increase continuously in the near future. This study investigates the response of the thermal regime to historical wetting in both permafrost and SFG areas and examines their relationships separately using the Community Land Surface Model version 4.5. Results show that wetting before the 1990s across the QTP mainly cooled the permafrost body in the arid and semiarid zones, with significant correlation coefficients of 0.60 and 0.48, respectively. Precipitation increased continually at the rate of 6.16 mm decade^{-1} in the arid zone after the 1990s but had a contrasting warming effect on permafrost through a significant shortening of the thawing duration within the active layer. However, diminished rainfall in the humid zone after the 1990s also significantly extended the thawing duration of SFG. The relationship between the ground thawing index and precipitation was significantly negatively correlated (−0.75). The dual effects of wetting on the thermal dynamics of the QTP are becoming critical because of the projected increases in future precipitation.

Key words: freezing/thawing indexes, numerical modeling, wetting process, frozen ground, Qinghai–Tibetan Plateau

Citation: Fang, X. W., Z. Li, C. Cheng, K. Fraedrich, A. Q. Wang, Y. H. Chen, Y. G. Xu, and S. H. Lyu, 2023: Response of freezing/thawing indexes to the wetting trend under warming climate conditions over the Qinghai –Tibetan Plateau during 1961–2010: A Numerical Simulation. *Adv. Atmos. Sci.*, **40**(2), 211−222, https://doi.org/10.1007/s00376-022-2109-z.

Article Highlights:

- Before the 1990s, wetting mainly imposed a cooling effect on permafrost areas.
- The continuous increase in rainfall since the 1990s has exerted a strong warming influence on permafrost, especially in arid zones.
- After the 1990s, wetting began to trigger a warming influence on the thermal regime of seasonally frozen ground.

1. Introduction

The Qinghai–Tibetan Plateau (QTP), the highest and largest permafrost zone in the mid-latitudes, is a region highly vulnerable to the effects of global climate change (Zhang et al., 2021). According to recent findings, the extent of permafrost and seasonally frozen ground (SFG, excluding glaciers and lakes) on the QTP is 1.06 million and 1.45 million km^2, respectively (Li et al., 2019). Permafrost degradation on the QTP in recent decades, attributable to climate change, has been widely documented

* Corresponding author: Xuewei FANG
Email: fangxw77@163.com

(Li et al., 2019). As an important terrestrial system that provides both positive and negative feedback to climate systems (Zhang et al., 2021), permafrost dynamics on the QTP, including the current state, future dynamics, historical changes, and implications, represent a critical topic because of the substantial impact on the East Asian monsoon and even the global climate system. In addition, the effects of changing climate on the spatial variability and temporal variations of frozen ground on the QTP and the associated thermal and hydrological consequences have been the focus of concerted research in recent decades (Kurylyk et al., 2014).

Previous studies focused on the effect of global warming on permafrost and the prediction of the future dynamics of frozen ground on the QTP (Wu et al., 2013; Qin et al., 2016; Biskaborn et al., 2019). An observational study has indicated that typical frozen ground in the central and eastern QTP has warmed at the rate of 0.47°C (10 yr)$^{-1}$, exceeding the value of 0.35°C (10 yr)$^{-1}$ of atmospheric warming (Fang et al., 2019). To better quantify the response of the thermal regime on the QTP to climate change and to project its future dynamics, the surface ground freezing index (GFI) and the ground thawing index (GTI) were defined according to surface ground temperature (Wu et al., 2013). In situ observations obtained from 1900–2017 indicate that the GFI and the GTI have both fluctuated remarkably since the early 2000s in the upper Yarlung Zangbo River Basin in the southern QTP (Liu et al., 2021). Furthermore, the two indexes also reflect clear spatial heterogeneity in that the GFI decreases more notably in permafrost areas and that the GTI shows greater increases in areas of SFG. This implies that the warming in permafrost regions is more pronounced in winter and that summer warming is more pronounced in SFG regions (Wu et al., 2018).

Owing to the sparse distribution of observing stations and the harsh natural conditions on the QTP, numerical modeling is deemed an effective tool for studying permafrost dynamics and the response of permafrost to a warming climate (Chang et al., 2018; Fang et al., 2021; Luo et al., 2021). Such studies consistently show that atmospheric warming is one of the dominant inducers of permafrost degradation on the QTP. However, owing to the increase in annual precipitation (AP) load in arid and high elevation areas (Zhang et al., 2021), the associated effects of AP change on the QTP cannot be neglected owing to the non-negligible impacts on the freeze/thaw status of frozen ground. Permafrost monitoring has indicated that an increase in AP triggers a cooling (heating) effect in the active layer in the frozen (thawed) season (Li et al., 2019), which has a critical impact on deepening the active layer thickness (Wu et al., 2013). Moreover, recent studies confirmed that precipitation across the QTP has maintained high levels since the 1990s (Fang et al., 2021; Zhang et al., 2021). For example, the average AP during 1998–2012 was 86 mm higher than the average AP during 1983–97 (Zhang et al., 2021). Also, the spatial distribution of the wetting trend of the QTP is heterogenous (Meng et al., 2018). The complexity of change in AP over the QTP is bound to play an important role in altering regional thermal regimes, in addition to the effects associated with atmospheric warming, and its impact should be more widely recognized (Zhang et al., 2021). Fortunately, observational studies have been conducted that suggest the potential existence of a consistent negative effect of wetting on permafrost degradation on the QTP. However, considering the limited number of observing stations, additional numerical studies of the region should be conducted. Recently, a relevant numerical experiment indicated that climate wetting reduces the thermal response of permafrost to warming, especially in arid and semiarid zones (Zhang et al., 2021). It deepens our understanding of permafrost responses to wetting across the QTP on a regional scale. However, given the climatic background, it is still essential to establish the response of SFG on the QTP to historical wetting and warming under the scenario of widespread permafrost retreat, to elucidate any differences in the response between permafrost and SFG to heterogeneous wetting on the QTP, and to establish which areas of the QTP might be most vulnerable.

This study addresses these issues by comparing the GFI and the GTI in permafrost and SFG areas on the QTP during 1961–90 and 1991–2010, using historical simulations of the Community Land Surface Model version 4.5 (CLM4.5). Additionally, the relationships between the average AP and both the GFI and the GTI in the permafrost and SFG areas on the QTP are also investigated.

The remainder of this paper is organized as follows. Section 2 describes the data and methods, including the selection of 1990 as pivotal year, Section 3 presents the spatial changes in AP and ground thermal indexes. A comprehensive discussion of relationships between AP and ground thermal indexes in different types of frozen soil is provided in section 4, before the conclusion and suggestions for future work are given in section 5.

2. Data and methodology

2.1. *Data*

To validate the reliability of numerical outcomes while calculating the GFI and the GTI using the soil thermal variable, this study used hourly observed soil temperature from seven observing stations located on the QTP: BJ, QOMS, SETORS, NADORS, NAMORS, QT01, and QT03 (Fig. 1). As members of the integrated land–atmosphere interaction observation network, the five observing stations (BJ, QOMS, SETORS, NADORS, and NAMORS) fully characterize the meteorological conditions and the vertical distributions of the soil layer over the QTP (Ma et al., 2020). For example, the NAMORS station is located on the banks of Lake Nam Co; the surrounding land is covered by alpine meadows, and the soil type is predominantly sandy silt loam. The QOMS station is situated at the bottom of the lower Rongbuk Valley; the surrounding surface is covered with sparse and short vegetation, and sand and gravel are predominant in the soil. Detailed information about each site can be

found in Ma et al. (2020). To guarantee the representativeness of the validation in the four climate zones, QT01 and QT03, located in the semiarid zone, are also used in this study (Zhao et al., 2021). In the permafrost zone of QTP, QT01 at Wudaoliang and QT03 at Beiluhe represent typical alpine meadow conditions with an average active layer thickness of 163 cm and 231 cm, respectively, from 2005–18. A detailed description of the sites can also be found in Zhao et al. (2021).

Although professional calibration and data consistency check procedures are applied to ensure the accuracy and reliability of the observational data before release, further procedures such as data selection and bias correction are also required (Ma et al., 2020; Zhao et al., 2021). In this study, the observed hourly soil temperature data were retained only if the record was available for an entire day (24 h), and individual soil layer data were accepted only if the record was complete for more than one year. Consequently, soil temperature data were available at different soil depths at BJ (4, 10, and 40 cm), QOMS (10, 40, 80, and 160 cm), SETORS (10, 20, 60, and 100 cm), NADORS (0, 20, 50, 100, and 200 cm), NAMORS (20, 40, 80, and 100 cm), QT01 (10, 50, 100, 160 cm), and QT03 (10, 50, 90, 200, 240 cm). For simplicity, the soil temperature values from individual observing stations were averaged for the shallow layer (depths above 20 cm) and the deep layer (depths below 40 cm). Simulation outcomes were also derived based on the observational depths and averaged using the same processing method for validation. Details regarding the stations and the observational data used in the study are presented in Table 1.

2.2. *Mathematical formulas and terms*

2.2.1. *Ground freezing/thawing indexes*

The GFI and the GTI are freezing and thawing indexes, respectively. The GFI can be conceptualized as the accumulated ground temperature in the whole freezing period from 1 July to 30 June in the next year. Similarly, GTI is the accumulated temperature in the whole thawing period from 1 January to 31 December within a calendar year (Yao et al., 2012; Qin et al., 2016; Liu et al., 2021):

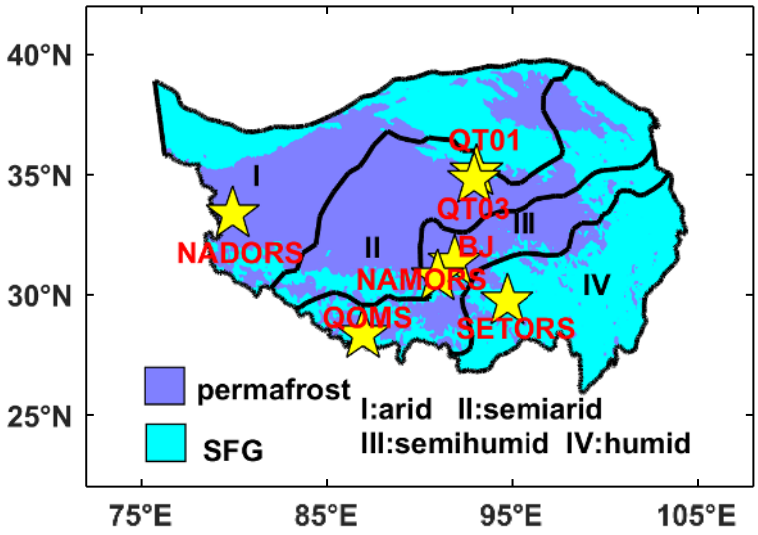

Fig. 1. Locations of the seven observing stations (stars) used in this study to validate the model outputs of soil temperature. Black lines outline the four dry–wet zones on the QTP. Colored shading depicts the distribution of the two types of frozen ground: seasonally frozen ground (SFG) and permafrost.

Table 1. Details of the soil temperature data from the seven observing stations and comparison of the correlation coefficient (Corr) and standard deviation (Std, °C) of the soil temperature in the shallow and deep layers between the observations and the CLM4.5 output for 2005–10. The * indicates the correlations with statistical significance at or above the 95% level.

Station	Latitude (°N)	Longitude (°E)	Elevation (m)	Period	Depth (cm)	Shallow layer		Deep layer	
						Corr	Std	Corr	Std
BJ	31.37	91.9	4509	2006–2010	4, 10, 40	0.77*	23.68	0.71*	20.43
QOMS	28.36	86.95	4298	2005–2010	10, 40, 80, 160	0.91*	23.71	0.90*	23.33
SETORS	29.77	94.73	3327	2007–2010	10, 20, 60, 100	0.92*	23.79	0.95*	15.08
NADORS	33.39	79.7	4270	2009–2010	0, 20, 50, 100, 200	0.72*	24.43	0.69*	23.15
NAMORS	30.77	90.98	4730	2005–2010	20, 40, 80, 100	0.93*	23.81	0.95*	23.22
QT01	35.14	93.04	4740	2005–2010	10, 50, 100, 160	0.81*	45.83	0.83*	35.97
QT03	34.82	92.92	4600	2005–2010	10, 50, 90, 200, 240	0.94*	14.69	0.82*	8.99

$$\mathrm{GFI} = \sum_{i=7}^{M_\mathrm{F}} |T_L\, D_i, \left(\overline{T_L} < 0^\circ\mathrm{C}\right), \quad (1)$$

$$\mathrm{GTI} = \sum_{i=1}^{M_\mathrm{T}} \left|\overline{T_L}\right| D_i, \left(\overline{T_L} > 0^\circ\mathrm{C}\right), \quad (2)$$

where $\overline{T_L}$ is the monthly surface ground temperature, and D_i represents the number of days in the i-th month. M_F represents those months with a negative mean monthly ground temperature from July to next June, and M_T represents months with a positive mean monthly temperature.

2.2.2. *Surface frost index*

In this study, a climate-based surface frost index (SFI) was used to diagnose the near-surface permafrost (Chang et al., 2018):

$$\mathrm{SFI} = \frac{\sqrt{\mathrm{DDF}^+}}{\sqrt{\mathrm{DDF}^+ + \sqrt{\mathrm{DDT}}}}, \quad (3)$$

where DDF+ and DDT are compound quantities that denote the multiplication of the annual number of freezing or thawing days by the air temperature (°C d), respectively. In this study, the annual surface air temperature series was numerically integrated using the monthly outputs of CLM4.5. The superscript (+) of DDF represents an adjustment for the effects of snowcover, using a negative exponential function depending on snow density, depth, and thermal conductivity (Nelson and Outcalt, 1987). The SFI values vary from 0 to 1, with sporadic permafrost indicated by 0.50–0.60, extensive permafrost by 0.60–0.67, and continuous permafrost indicated by values above 0.67 (Slater and Lawrence, 2013). In this study, a threshold value of 0.58 was used to diagnose permafrost, i.e., SFI ⩾ 0.58 was taken to indicate the existence of continuous permafrost area, which has been confirmed by Slater and Lawrence (2013) matching the observed permafrost area by using a minimum frost index value of 0.58.

2.2.3. *Model and numerical simulation design*

The CLM4.5 model has been widely employed to study the permafrost dynamics of the QTP (Xie et al., 2017; Fang et al., 2021; Luo et al., 2021), and it was adopted in this study to obtain the essential dataset of soil temperatures. The CLM model simulates the partitioning of mass and energy from the atmosphere, redistributes the mass and energy of the land surface, and then exports the fresh water and heat to the ocean (Swenson and Lawrence, 2012). It is the land component of the Community Climate System Model and the Community Earth System Model (Lawrence et al., 2011). Detailed information on CLM4.5 can be found in the Technical Description published by the National Center for Atmospheric Research (Oleson et al., 2013).

Driven by a high-resolution atmospheric dataset (temporal resolution: 3 h, spatial resolution: 1 km) released by the Beijing Normal University (China, hereafter BNU), the numerical simulation in this study was conducted for the period 1961–2010 with a spatial resolution of 0.05° × 0.05° and the numerical output was set to a monthly timestep (Fang et al., 2021). As one of the seven essential meteorological factors to drive the model, the precipitation amount across the QTP used in this study was also derived from the BNU dataset. Gauge observations and satellite estimates of daily precipitation are two primary inputs to the merged analysis of the dataset. Although the dataset has shown superior performance in representing the spatiotemporal variations of precipitation over most regions, unrealistic distribution patterns are also observed in the analysis over western China because of the spurious extrapolation of heavy rainfall at isolated stations (Xie and Xiong, 2011). In this study, the reliabilities of the atmospheric forcing dataset (air temperature and precipitation) and outputs (soil temperature and soil moisture) have been validated in previous work using in situ observations (Li et al., 2014; Fang et al., 2021).

2.2.4. *Partitioning of the study area*

To quantify the different responses of SFG and permafrost to wetting, a climate classification and the average AP were used to divide the entire QTP into four subregions: the arid zone (I, AP < 200 mm), semiarid zone (II, AP: 200–400 mm), semihumid zone (III, AP: 400–800 mm), and humid zone (IV, AP > 800 mm), as shown in Fig. 1 (Gao et al., 2015; Zhang et al., 2021).

2.2.5. *Partitioning of the time series*

Gao et al. (2014) reported that the observed annual surface air temperature and precipitation averaged across the QTP showed abrupt changes around 1998. Especially since 1998, the AP has maintained high levels and peaked in 2005 (Zhang et al., 2021). In this study, abrupt changes in annual air temperature and precipitation across the QTP occurred in 1991 and 1984, respectively, as determined by the Mann-Kendall test from the BNU (Mann, 1945; Kendall and Gibbons, 1990). In comparison to the period of 1961–90, the 1991–2010 averages of annual air temperature and precipitation over the QTP increased dramatically by 0.72°C and 75.64 mm, respectively (Fig. 2a). The annual air temperature and AP in the four dry–wet zones show prevailing warming trends throughout the QTP, especially in the arid zone (Fig. 2b). However, the temporal patterns of AP in dry–wet zones show remarkable differences in their tendencies, that is, the arid and semiarid zones became warmer and wetter in the period 1991–2010, relative to 1961–90 (Figs. 2b, c); while the climate conditions over the humid and semihumid zones became warmer but drier (Figs. 2d, e). By contrasting the annual air temperature and AP averaged across the QTP, it is clear that air temperature and AP increased substantially from 1991–2010 (Fig. 2a). Therefore, we divided the entire period from 1961 to 2010 into two phases, i.e., 1961–90 and 1991–2010, with 1990 as the pivotal year.

3. Results

3.1. *Model validation using observations*

Although the reliability of soil temperature and soil mois-

ture has been validated using field observations from 14 sites across the QTP at depths of 10, 40, and 160 cm (Fang et al., 2021), it is also useful to verify the model performance in four climate zones. As shown in Fig. 3, the simulated soil temperature fits well with the data from the seven observing stations. Statistically, the correlation coefficient (Corr) between soil temperature is significant at 0.69 at NADORS and 0.95 at both SETORS and NAMORS in the deep layer; the standard deviation (Std) is between 8.99°C at QT03 in the deep layer and 45.83°C at QT01 in the shallow layer (Table 1). The simulated scatterplots tend to reflect the observations well, especially at QT03 and NAMORS in the shallow layer (Fig. 3a). The simulations at SETORS and NADORS also produce Corr values of 0.92 and 0.72, respectively, for the shallow layer, although the numerical temperatures are slightly warmer than the observed soil temperatures. Regionally, the model tends to yield better performance for the upper layer soil temperatures in the semihumid zone (Fig. 1). Similarly, the simulated soil temperatures are also comparable with the observed temperatures in the deep layer with Corr values of 0.69–0.95 (Table 1). For SETORS, the Corr is 0.95, and the Std is 15.08°C; however, the model tends to overestimate the soil temperature relative to the observations (Fig. 3b). For both BJ, QOMS, and QT03, the

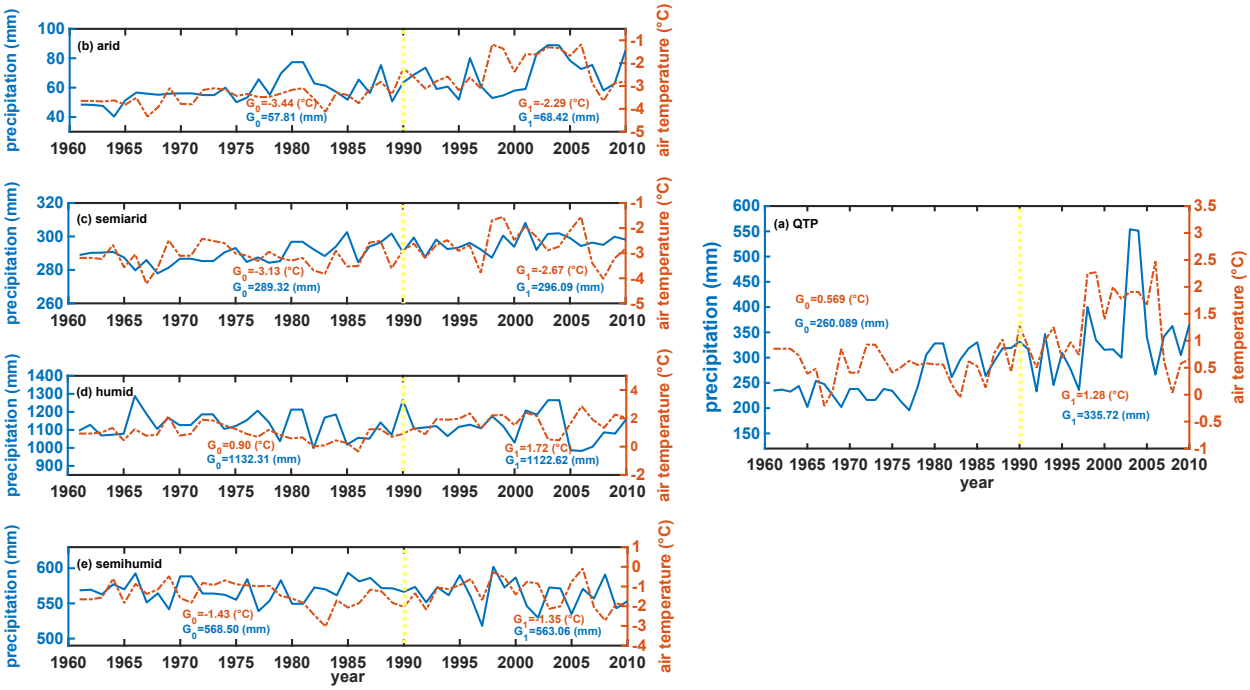

Fig. 2. Time series of air temperature (red color) and precipitation (blue color) in the four dry–wet zones on the QTP. Averaged air temperature and precipitation during 1961–90 (G_0) and 1991–2010 (G_1) are shown in the panel in the (a) entire QTP, (b) arid zone, (c) semiarid zone, (d) humid zone, and (e) semihumid zone. The vertical lines (yellow color) mark 1990, the pivotal year in this study.

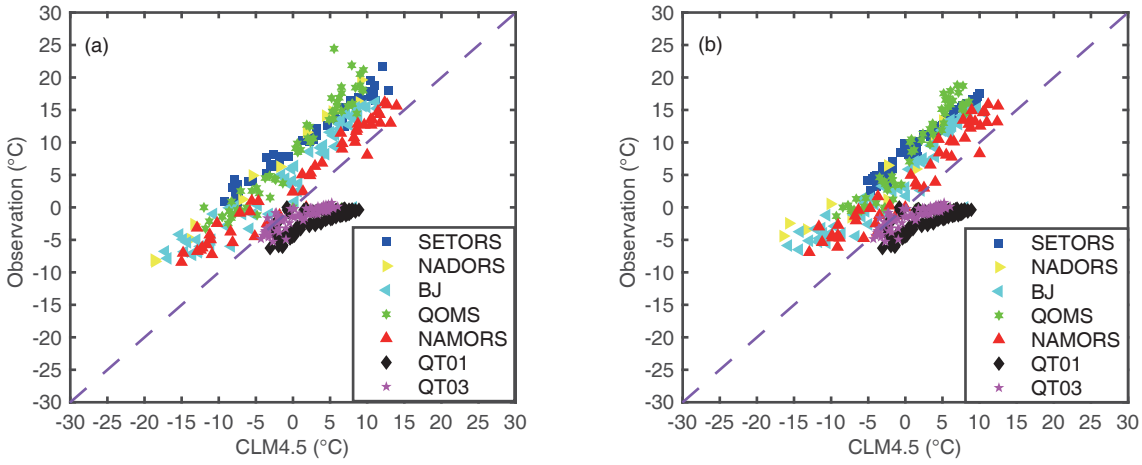

Fig. 3. Comparison of simulated and observed temperatures in the shallow layer (a) (depth above 20 cm) and deep layer (b) (depth below 40 cm) soil layer at the seven observing stations in four dry–wet zones across the QTP.

model performs better for the deep layer than for the upper layer, as evidenced by the more concentrated nature of the scatterplot (Fig. 3b). In comparison with the deep layer, validation of the accuracy for the shallow layer might be limited by data availability and quality, as shown in Table 1. Overall, the average Corr and Std values between the observations and simulated soil temperatures among the seven observing stations are 0.85 and 23.58°C, respectively. This means that the simulated outcomes can be readily accepted as a basic dataset to investigate the GFI and the GTI across the QTP.

3.2. *Climatology of the GFI and the GTI on the QTP*

As the 1990s represent the pivotal period of wetting, the spatial patterns of the climatology of the GFI and the GTI on the QTP since the 1990s are shown in Figs. 4a and 4b, respectively. In the western and northern parts of the QTP, the climatology of the GFI and the GTI tend to show opposite patterns under the background of wetting. For the GFI, higher values are evident in the alpine permafrost area of the western QTP and the northern Qilian Mountains. However, the GTI has lower values in those areas but higher values in both the Qaidam Basin and the western and eastern edges of the QTP. In the eastern QTP, the GFI is consistent with the GTI in that they both have lower values (Figs. 4a, b), implying that the freezing and thawing intensity is weak in lower altitude regions. From the perspective of magnitude, the maximum value of the GTI shown in Fig. 4b is >3500°C d, which is substantially higher than that of the GFI. It shows that the thawing process of soil has played a dominant role in the QTP since the 1990s.

We also investigated the spatial difference ratios of the GFI and the GTI of the two subperiods, i.e., the differences between two temporal series: 1991–2010 and 1961–90 were divided by the values from 1961–90 (Figs. 4c, d). As shown in Fig. 4c, the difference ratios of GFI are mostly lower than zero across the entire QTP, and the largest values are concentrated in the northern and the southern parts of the QTP, which are classified as arid and semihumid regions in terms of their AP. The remarkable decreases in the GFI indicate the surface ground has warmed substantially since the 1990s. Figures 2b and 2e show that the arid regions have undergone wetting and warming climate conditions since the 1990s, whereas the semihumid zone underwent warming but also drying conditions during this period. The dramatic warming in these two zones illustrates the different roles of air temperature and precipitation on the thermal regimes in dry and wet environments. Yin and Roderick (2020) reported that variations in near-surface air temperature are independent of precipitation in wet environments but respond strongly to precipitation variations in dry environments by altering the surface radiation components. Based on these conclusions, the dramatically decreasing GFI and increasing GTI in the arid zone (Figs. 4c, d) are closely related to the wetting, which has exerted an important warming impact on the ground. This lies in contrast to the semihumid zone, where the remarkable decreases in GFI were induced by the air warming, while variations in AP would mostly leads to variable runoff common to wetter environments (Yin and Roderick, 2020).

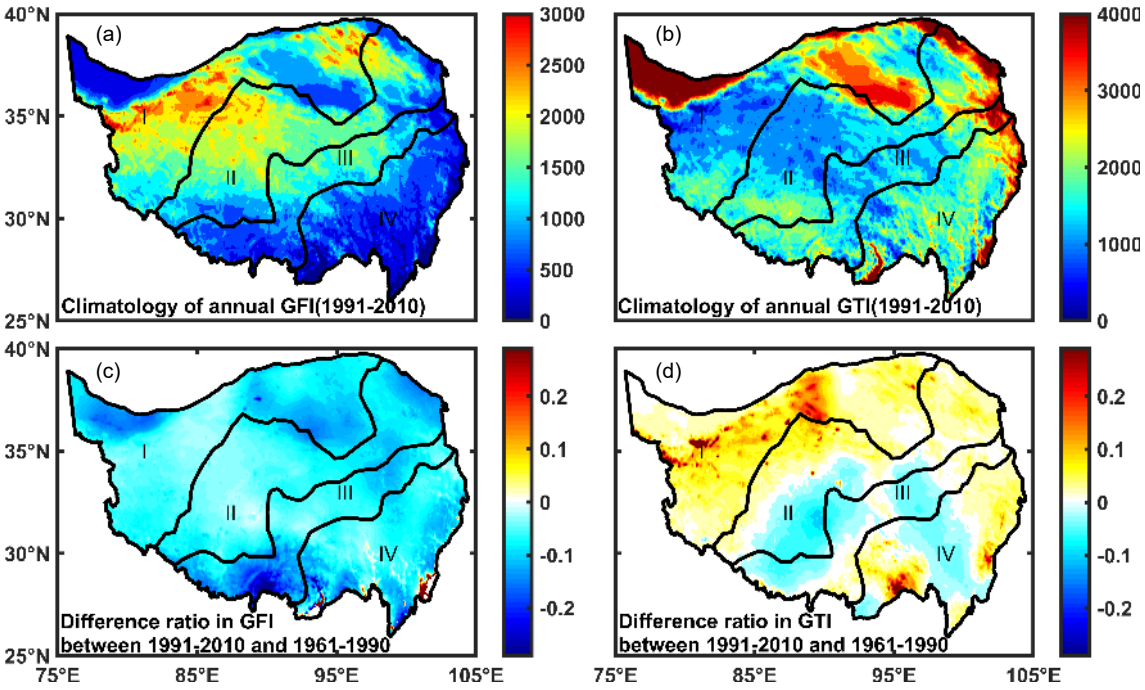

Fig. 4. Climatology of the (a) annual mean GFI (°C d) and (b) annual mean GTI (°C d) from 1991–2010, and the spatial difference ratios of (c) the GFI and (d) the GTI between 1991–2010 and 1961–90. The maps also show the four dry–wet zones (I–IV) of the QTP.

The positive-dominated difference ratios of the GTI between 1991–2010 and 1961–90 reflect the accelerated reaction of the ground to regional warming and wetting (Fig. 4d). Distinct regional differences in the GTI are evident in the arid and semiarid zones of the QTP, which represent the main permafrost areas of the QTP (Fig. 1). The largest positive difference ratios of the GTI exist in the arid zone (Fig. 4d), while distinct negative difference ratios are evident in the semiarid zone under the background of the increase in AP since the 1990s (Fig. 2c). It means that a tendency of transition of SFG to permafrost occurs in the southwestern QTP (Fig. 1). Following sensitivity experiments, Zhang et al. (2021) declared that summer precipitation exerts a strong cooling effect on the frozen ground in the semiarid zone of the QTP. Compared to the warming effect in the arid zone, the wetting effect exerted on the ground is characterized by intensively negative difference ratios of the GFI but positive difference ratios of the GTI (Figs. 4c, d). This verifies the conclusion by Zhang et al. (2021), further confirming that the thermal response of frozen ground to wetting depends on precipitation amounts in both arid and semiarid zones.

3.3. *Spatial changes of GFI, GTI, and precipitation*

The changes of the GFI and the GTI, which illustrate variations in the duration of freezing and thawing in surface ground soil, show distinctive regional differences in the historical periods across the QTP (Fig. 5) that are suggestive of differing responses of permafrost and SFG to wetting and warming in the different dry–wet zones. However, to the best of our knowledge, this has received little attention in previous studies. The highest increases in the GFI and the GTI during 1961–90 are evident in the arid and semiarid zones in the permafrost region (Figs. 5a, c, respectively), as indicated by the dynamics of the permafrost distribution (Figs. 5h, i). Meanwhile, decreasing trends in these indexes are also evident in the SFG of the eastern QTP (Figs. 5a, c). From 1961–90, the GFI and the GTI increased with rates of 28.07 and 7.34°C d (10 yr)$^{-1}$, respectively, in permafrost areas but decreased in SFG areas with respective rates of 14.17 and 19.27 °C d (10 yr)$^{-1}$ (Table 2). This finding implies that the

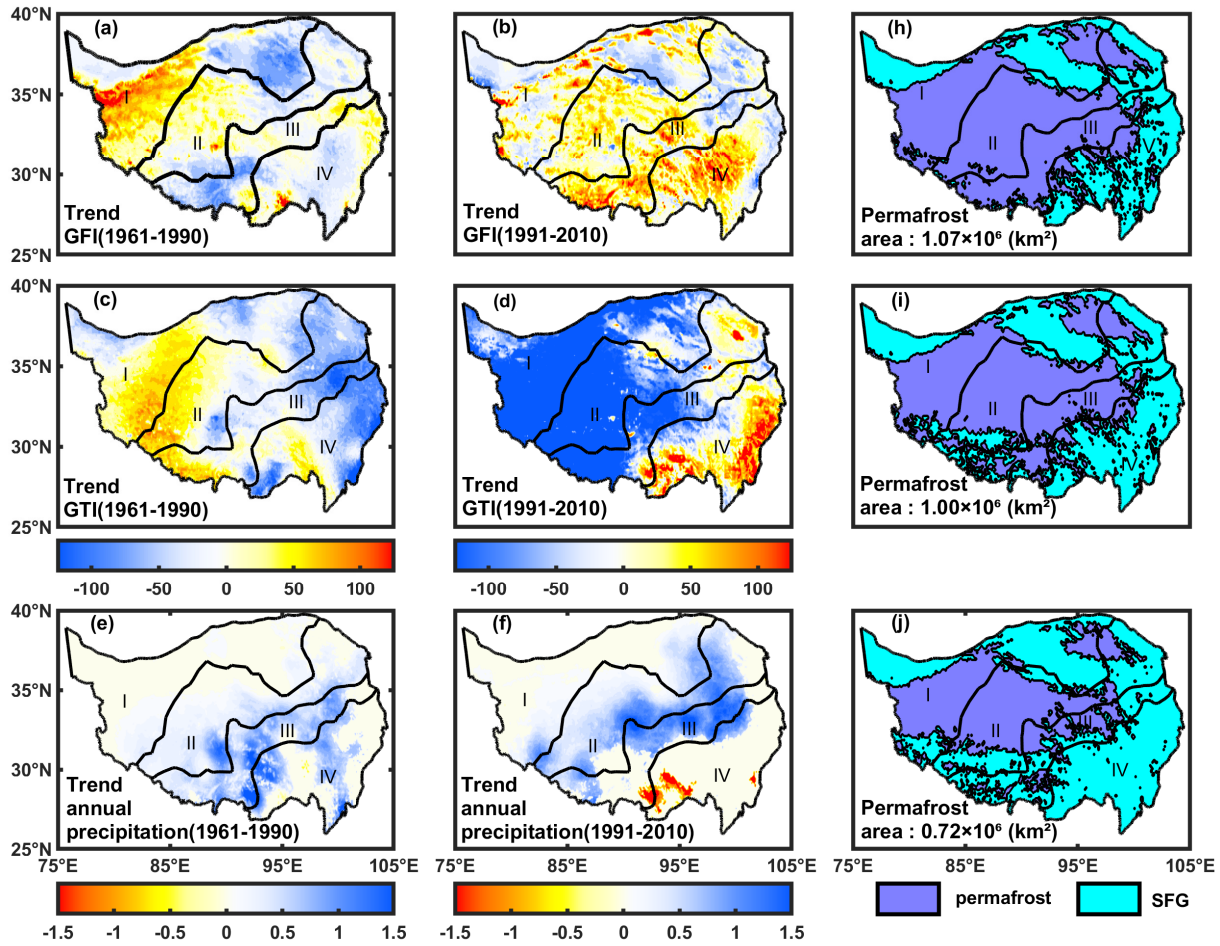

Fig. 5. Comparison of spatial trends [°C d (10 yr)$^{-1}$] of averaged annual GFI and GTI from 1961–90 (a and c, respectively) and 1991–2010 (b and d, respectively). The spatial trend of annual precipitation [mm d^{-1} (10 yr)$^{-1}$] is also shown: (e) from 1961–90 and (f) from 1991–2010. Accordingly, the distributions of permafrost (SFI ≥ 0.58) and SFG (SFI < 0.58) defined by the SFI across the QTP are displayed: (h) in 1961, (i) in 1990, and (j) in 2010. Regions I–IV correspond to the arid zone, semiarid zone, semihumid zone, and humid zone, respectively.

Table 2. Comparison of the annual trends of the GFI, GTI, and annual precipitation (AP) over the entire QTP in the permafrost and SFG regions during 1961–90 and 1991–2010. The * indicates the trends statistically significant at or above 95% level.

Trend	Region	Periods	
		1961–90	1991–2010
GFI [°C d (10 yr)$^{-1}$]	QTP	7.47	30.90
	Permafrost	28.07	50.48
	SFG	–14.17	–31.90
GTI [°C d (10 yr)$^{-1}$]	QTP	–7.31	–57.33
	Permafrost	7.34	–105.56
	SFG	–19.27	–4.11
AP [mm (10 yr)$^{-1}$]	QTP	34.26*	27.59
	Permafrost	34.56*	50.50*
	SFG	35.42*	14.49

freezing (thawing) duration in permafrost (SFG) areas of the QTP is more vulnerable to climate change. Permafrost tends to freeze slowly in the active layer, whereas SFG tends to thaw rapidly in the frozen layer in response to climatic change. Zhang et al. (2021) confirmed that increased precipitation triggers strong cooling effects upon the frozen ground of arid and semiarid zones. The marked increase in AP across the QTP during the study period (Fig. 5e, Table 2) might have induced the increase in GFI values in these permafrost zones. However, in the warmer and wetter SFG areas, because the near-surface air temperature (and also the surface energy balance) is not particularly sensitive to variations in AP, precipitation primarily acts as a source of variation for runoff (Yin and Roderick, 2020). Liquid water percolating into the soil depths provides massive heat input (Zhang et al., 2021), thus markedly shortening the thawing duration, evidenced by GTI rate decreases of up to 19.27°C d (10 yr)$^{-1}$, especially in the semihumid and humid zones (Fig. 5c). These results suggest that the increase in precipitation across the QTP during 1961–90 might have exerted contrasting effects on the permafrost and SFG in different dry–wet zones owing to the different responses of the near-surface air temperature and surface energy components to variations in AP in wet and dry environments (Yin and Roderick, 2020).

The comparison of the spatial changes of precipitation since the 1990s reveals that precipitation has increased substantially, but with greater regional differences (Fig. 5f). Areas with high values of precipitation increases have expanded from the semihumid zone into the semiarid zone since the 1990s. However, the humid zone, classified as SFG at the end of the study period, shows a dramatic decrease in precipitation, especially in the region of the Tanggula and Hengduan mountains. Zhou et al. (2019) showed that the water vapor flux at the eastern boundary of the QTP decreased after 1994, which might be related to the drying process that occurred in the humid areas of the QTP. Notably, the intense wetting process over the QTP has been concentrated mainly in permafrost regions, with a trend of 50.50 mm (10 yr)$^{-1}$, significant at the 95% confidence level (Table 2). A massive precipitation load in cold and dry permafrost areas can substantially alter soil thermal regimes (Lupascu et al., 2014). Substantial rainfall can percolate into the active layer of permafrost, delivering heat and warming the deep soil, as evidenced by the remarkable declines in the GTI shown in Fig. 5d. The modeling in this study shows that the GTI decreased at the rate of 105.66 °C d during 1991–2010 (Table 2), implying that the thawing process of the active layer in permafrost areas has accelerated tremendously. Although the freezing duration has also been extended to some extent owing to the accumulation of liquid water in the upper soil of the permafrost, as evidenced by the increase in the GFI (Fig. 5b), the warming effect of heat exchange that accompanies abundant rainfall percolating into the deep soil acts as a pivotal positive factor in permafrost dynamics. Zhang et al. (2021) confirmed that a wetting of 100 mm results in the reduction of the active layer thickness by 0.35 m and warms the top of the permafrost by 0.36°C. The results of this study further confirm that the wetting associated with the increased precipitation load since the 1990s has caused warming and accelerated the thawing process within the active layer. Consequently, the permafrost area shrank from 1.00×10^6 km^2 to 0.72×10^6 km^2 at the end of the study period, especially in the alpine permafrost region of the southwestern QTP (Fig. 5j).

The decline in precipitation in the humid zone probably exerted a different effect on SFG. A diminished precipitation load decreases the amount of water percolating into the deep soil, leading to water accumulation and enhanced freezing in the upper soil. This is evidenced by the obvious increase in the GFI values in the humid zone, as shown in Fig. 5b. At a time when phase changes are occurring within the frozen layer, heat consumption will be increased markedly by surface evaporation, leading to an extension of the thawing duration, as shown by the increase in the GTI values in Fig. 5d. We can conclude from these results that the uneven increase in precipitation across the QTP has exerted an accelerating effect on permafrost thawing; however, it has the opposite effect in the humid zone in the presence of SFG.

4. Discussion

4.1. *Anomalies and trends of precipitation, GFI, and GTI in dry–wet zones*

The impact of wetting on the thermal regime of frozen soil on the QTP varies depending on the climate zone. Therefore, it is necessary to quantify the anomalies and trends of the GFI, GTI, and precipitation for each zone separately to detect the areas susceptible to the most sensitive responses. As shown in Table 3, the AP has increased consistently in all four climate zones, with a trend of 0.58–5.18 mm (10 yr)$^{-1}$ before the 1990s, and most variations, as indicated by the largest magnitude of anomalies (Fig. 6c), occurred in the humid zone. Table 3 shows that precipitation in the humid

zone increased (by 5.18 mm (10 yr)$^{-1}$) before the 1990s, while it turned decreasing dramatically (20.10 mm (10 yr)$^{-1}$) since the 1990s to the end of the study period. Furthermore, as the zones that account for 60% of the total permafrost area of the QTP (Zhang et al., 2021), the arid and semiarid zones show larger magnitudes of change in the GFI than in the GTI, which indicates that the primary effects of wetting on freezing duration occur in the early wetting stage. Positive values of change in the GFI also indicate the cooling effects of wetting in these cold and dry zones.

The steady increase in precipitation since the 1990s, especially in the arid zone (6.16 mm (10 yr)$^{-1}$, Fig. 6c, Table 3), has exerted an impressive negative impact on the GTI. It implies that the constantly increasing precipitation load has changed from exerting a cooling effect to exerting a warming effect on the permafrost in the arid zone. Numerical experiments indicated that the increase in the cooling effect in the arid zone is halted when the increase in the annual precipitation exceeds 100 mm (Zhang et al., 2021). The results of this study further suggest that an intensive precipitation load not only diminishes the cooling effect but also accelerates the thawing process occurring within the active layer of permafrost, as evidenced by the sizable decline in the GTI and the weaker increase in the GFI shown in Table 3.

Conversely, precipitation in the semihumid and humid zones increased substantially during 1961–1990 but exhibited the opposite trend thereafter. The semihumid and humid zones were originally characterized as typical areas of permafrost and SFG, respectively, before the 1990s (Figs. 5h, i). From the higher values of the trend of the GTI compared with those of the GFI in these zones (Table 3), it can be concluded that the thawing process has displayed a marked response to the wetting and that the most obvious warming effects have occurred in the humid zone, as evidenced by the substantial decline in the GTI [117.31 °C d (10 yr)$^{-1}$, Table 3]. Nevertheless, with the progressive decrease in precipitation since the 1990s, the greatest negative anomaly in precipitation was also detected in the humid zone (Fig. 6c). The GTI values in this zone, however, yield a positive anomaly and trend during this period, contrary to those in the other three zones. As the typical SFG on the QTP, the most obvious drying in the humid zone has been coupled with the tremendous extent of the delay in the thawing process. Decreased precipitation and the resulting reduction in

Table 3. Comparison of trends in the GFI, GTI, and annual precipitation in different dry–wet climate zones of the QTP from 1961–90 and 1991–2010. The * indicates the trends with statistical significance at or above the 95% level.

Trend	Climate Zone	Period	
		1961–1990	1991–2010
GFI [°C d (10 yr)$^{-1}$]	arid	41.39	33.29
	semi-arid	81.14*	96.68
	semi-humid	69.88*	119.81
	humid	28.14	11.86
GTI [°C d (10 yr)$^{-1}$]	arid	27.61	–110.24
	semi-arid	–45.79	–62.23
	semi-humid	–83.03*	–64.04
	humid	–117.31*	67.92
Annual Precipitation [mm (10 yr)$^{-1}$]	arid	5.17*	6.16
	semi-arid	3.41*	2.88
	semi-humid	0.58	–4.44
	humid	5.18	–20.10

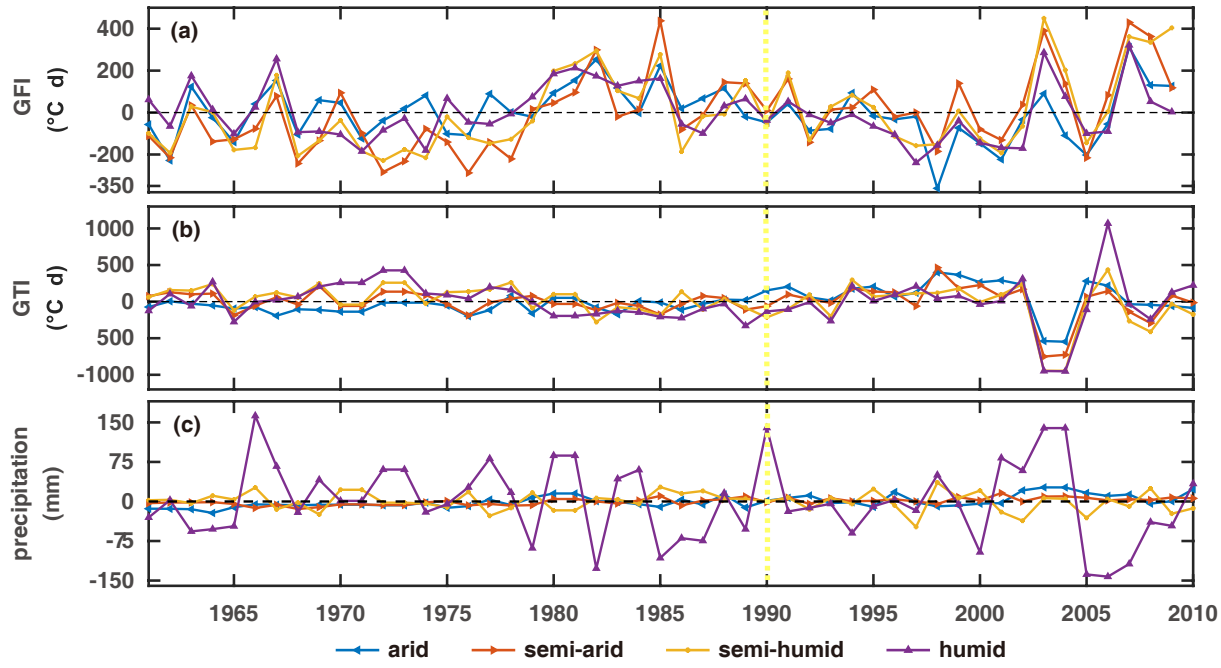

Fig. 6. Comparison of anomalies in (a) the GFI, (b) the GTI, and (c) precipitation in the arid, semiarid, semihumid, and humid zones from 1961–2010. The vertical shading marks the pivotal year 1990, which divides the two subperiods.

soil moisture in the surface layer might restrict the transfer of heat to the deeper layer when phase change occurs. Meanwhile, owing to the absence of the continuous increase in precipitation, the previous cooling effect of wetting on the permafrost in the semihumid zone might have become further enhanced since the 1990s, as evidenced by the larger positive anomaly and trend of the GFI shown in Fig. 6a. Massive thermal degradation in the semihumid zone might have slowed during this period. These results indicate that the thermal regime of the arid and humid zones shows the most obvious response to wetting due to their greater vulnerability to the thawing duration. Wetting over the QTP tends to exert dual effects on permafrost that depend on the precipitation amount while exerting a warming effect on SFG.

4.2. *Correlation analysis between precipitation and both the GFI and the GTI in different types of frozen soil*

The results of the correlation analysis (Corr) between precipitation and the thermal indicators (GFI and GTI) are listed in Table 4 to demonstrate the dependence on both the permafrost and seasonally frozen ground regimes and on the effect of dry and wet conditions (zones) to elucidate the diversity of the responses to wetting. Results show that the Corr between AP and the GFI is significant only in the arid zone of the permafrost area before the 1990s (Corr = 0.60, Table 4). The substantial increase in AP in the arid zone during 1961–90, shown in Fig. 2b and Table 3, means that the wetting process tends to induce an extension of the freezing duration within the active layer in the permafrost region. Observations generally show a negative correlation between the near-surface air temperature and AP in dry environments (Yin and Roderick, 2020). Dramatic wetting over cold and arid permafrost zones tends to induce a cooling of the atmosphere (averaged as –3.44°C, shown in Fig. 2b), thus inducing a strong cooling effect on permafrost in the arid zone. Wetting also significantly affected the thawing duration of permafrost in the semiarid zone, as evidenced by the positive Corr of 0.48 (Table 4). The surface energy balance responds strongly to variations in AP by altering the surface radiation components and latent and sensible heat fluxes, which can alter the near-surface air temperature (Yin and Roderick, 2020). Hence, in dry areas, the surface ground heat loss occurs inevitably under both cooling and wetting conditions (Fig. 2c and Table 3) and reduces the heat transferred to the deeper layer and thus increasing the thawing duration.

Table 4. Comparison of correlation coefficients between the GFI, GTI, and annual precipitation in permafrost and SFG from 1961–2010 on the QTP. The * indicates correlations that are statistically significant at or above 95% level.

			Periods	
Variable	Frozen Type	Climate Zone	1961–1990	1991–2010
GFI (°C d)	Permafrost	arid	0.60*	0.24
		semiarid	0.05	–0.29
		semihumid	0.29	0.15
		humid	–0.08	–0.16
	SFG	arid	0.05	–0.40
		semiarid	0.09	–0.31
		semihumid	–0.16	0.05
		humid	0.34	0.26
GTI (°C d)	Permafrost	arid	–0.08	–0.71*
		semiarid	0.48*	0.45
		semihumid	0.13	–0.41
		humid	–0.31	–0.24
	SFG	arid	–0.03	–0.49*
		semiarid	–0.34	–0.13
		semihumid	–0.17	0.22
		humid	0.21	–0.75*

Since the 1990s, wetting has shown distinctive regional differences across the QTP, manifested primarily as a trend of further wetting in the arid and semiarid zones. In contrast, the opposite trend occurred in the humid and semihumid zones (Fig. 2 and Table 3). In the arid zone of permafrost, AP is mainly negatively correlated with the GTI. The continuous wetting in the arid zone since the 1990s shortens the thawing duration substantially and thus imparts a strong warming effect on the permafrost body. In the SFG, however, changing precipitation mainly influences the thawing duration in the arid and humid zones. In the arid zone, enhanced rainfall accelerates the thawing stage in the frozen layer, as indicated by the negative Corr of –0.49 shown in Table 4. It can be concluded that wetting exerts strong warming effects on the thermal regime of the SFG in the arid area. Nevertheless, declining precipitation in the humid zone tends to trigger a prolonged thawing of the SFG, as evidenced by the strikingly negative Corr between rainfall and the GTI (–0.75, significant at the 95% confidence level). This can be explained by a diminished percolation of liquid water and thus a reduced heat transport to deeper layers. The accumulation of water and enhanced soil moisture in the surface layer leads to greater heat loss via evaporation. Consequently, when the thawing process occurs, it takes longer for the deeper soil to accumulate the sufficient latent heat required for the melting of ice.

5. Conclusions

Regional variations in the surface ground freezing index (GFI) and the ground thawing index (GTI) and their response to wetting during 1961–2010 were analyzed using numerical methods. The following conclusions are drawn from the results:

(i) Wetting across the QTP before the 1990s has affected the permafrost area. Enhanced rainfall exerts a cooling on the permafrost body, but in different climate zones, it correlates differently with thermal indicators. In arid zones, wetting extends the freezing duration within the active layer, while in semiarid zones, it prolongs the thawing period.

(ii) Permafrost and seasonally frozen ground (SFG) have been affected differently by wetting (since the 1990s). The arid and semiarid zones exhibited an increasing trend in

precipitation [6.16 and 2.88 mm (10 yr)$^{-1}$], whereas the semihumid and humid zones featured decreasing trends in precipitation [4.44 and 20.10 mm (10 yr)$^{-1}$]. In arid zones, a further increase of rainfall strongly affected the reduction of thawing periods in both the permafrost and seasonal frozen ground areas (evidenced by significant rainfall–GTI correlations), while in the humid zone, reduced precipitation has significantly extended the thawing state of seasonally frozen ground. In humid zones, a drying and warming environment tends to enhance heat loss at the ground surface. The consequent decrease in heat absorption, thus the insufficient latent heat supply for ice melting below the surface extends the thawing process.

Precipitation over the QTP is projected to increase in the future. Thus, the dual effect of wetting becomes a critical factor in determining the thermal dynamics of permafrost and seasonally frozen ground areas. Prolonged freezing durations and reduced thawing periods are expected with further increases in precipitation on frozen ground. To obtain a quantitative dynamical concept or develop a theoretical model, further research on these complex interactions of energy and water fluxes in the permafrost and seasonally frozen ground regimes is required.

Acknowledgements. We gratefully acknowledge in situ data support from the Institute of Tibetan Plateau Research, Chinese Academy of Science (https://doi.org/10.1922/sciencedb.00103), and the National Tibetan Plateau Data Center (http://data.tpdc.ac.cn/zh-hans/data/789e838e-16ac-4539-bb7e-906217305a1d/?q=2002-2018). This work was supported by the National Natural Science Foundation of China (Grant Nos. 41905008, 41975007, and 42075081) and the Innovation and Entrepreneurship Training Program for College Students of Chengdu University of Information Technology (CUIT) (202210621003, 202210621039, 202110621015). Additional support was provided by the Scientific Research Foundation of CUIT (KYTZ202126). We thank the Max Planck Institute of Meteorology (Atmosphere in the Earth System) for providing hospitality and support.

REFERENCES

Biskaborn, B. K., and Coauthors, 2019: Permafrost is warming at a global scale. *Nature Communications*, **10**, 264, https://doi.org/10.1038/s41467-018-08240-4.

Chang, Y., S. Lyu, S. Q. Luo, Z. G. Li, X. W. Fang, B. L. Chen, R. Q. Li, and S. Q. Chen, 2018: Estimation of permafrost on the Tibetan Plateau under current and future climate conditions using the CMIP5 data. *International Journal of Climatology*, **38**, 5659–5676, https://doi.org/10.1002/joc.5770.

Fang, X. W., S. Q. Luo, and S. H. Lyu, 2019: Observed soil temperature trends associated with climate change in the Tibetan Plateau, 1960–2014. *Theor. Appl. Climatol.*, **135**, 169–181, https://doi.org/10.1007/s00704-017-2337-9.

Fang, X. W., S. Q. Luo, S. H. Lyu, C. Cheng, Z. G. Li, and S. B. Zhang, 2021: Numerical modeling of the responses of soil temperature and soil moisture to climate change over the Tibetan Plateau, 1961–2010. *International Journal of Climatology*, **41**, 4134–4150, https://doi.org/10.1002/joc.7062.

Gao, Y. H., L. Cuo, and Y. X. Zhang, 2014: Changes in moisture flux over the Tibetan Plateau during 1979–2011 and possible mechanisms. *J. Climate*, **27**, 1876–1893, https://doi.org/10.1175/JCLI-D-13-00321.1.

Gao, Y. H., X. Li, L. R. Leung, D. L. Chen, and J. W. Xu, 2015: Aridity changes in the Tibetan Plateau in a warming climate. *Environmental Research Letters*, **10**, 034013, https://doi.org/10.1088/1748-9326/10/3/034013.

Kendall, M. G., and J. D. Gibbons, 1990: *Rank Correlation Methods*. 5th ed. Edward Arnold, 212pp.

Kurylyk, B. L., K. T. B. MacQuarrie, and J. M. McKenzie, 2014: Climate change impacts on groundwater and soil temperatures in cold and temperate regions: Implications, mathematical theory, and emerging simulation tools. *Earth-Science Reviews*, **138**, 313–334, https://doi.org/10.1016/j.earscirev2014.06.006.

Lawrence, D. M., and Coauthors, 2011: Parameterization improvements and functional and structural advances in Version 4 of the Community Land Model. *Journal of Advances in Modeling Earth Systems*, **3**, M03001, https://doi.org/10.1029/2011MS00045.

Li, D. S., Z. Wen, Q. G. Cheng, A. G. Xing, M. L. Zhang, and A. Y. Li, 2019: Thermal dynamics of the permafrost active layer under increased precipitation at the Qinghai-Tibet Plateau. *Journal of Mountain Science*, **16**, 309–322, https://doi.org/10.1007/s11629-018-5153-5.

Li, T., and Coauthors, 2014: Mapping near-surface air temperature, pressure, relative humidity and wind speed over Mainland China with high spatiotemporal resolution. *Adv. Atmos. Sci.*, **31**, 1127–1135, https://doi.org/10.1007/s00376-014-3190-8.

Liu, L., D. L. Luo, L. Wang, Y. D. Huang, and F. F. Chen, 2021: Dynamics of freezing/thawing indices and frozen ground from 1900 to 2017 in the upper Brahmaputra River Basin, Tibetan Plateau. *Advances in Climate Change Research*, **12**, 6–17, https://doi.org/10.1016/j.accre.2020.10.003.

Luo, J. X., S. H. Lyu, X. W. Fang, and Y. G. Liu, 2021: Trends in the frozen ground temperature on the Tibetan Plateau simulated by RegCM4.7-CLM4.5. *Theor. Appl. Climatol.*, **145**, 891–901, https://doi.org/10.1007/s00704-021-03664-3.

Lupascu, M., J. M. Welker, U. Seibt, K. Maseyk, X. Xu, and C. I. Czimczik, 2014: High Arctic wetting reduces permafrost carbon feedbacks to climate warming. *Nature Climate Change*, **4**, 51–55, https://doi.org/10.1038/nclimate2058.

Ma, Y. M., and Coauthors, 2020: A long-term (2005–2016) dataset of hourly integrated land-atmosphere interaction observations on the Tibetan Plateau. *Earth System Science*

Data, **12**, 2937–2957, https://doi.org/10.5194/essd-12-2937-2020.

Mann, H. B., 1945: Nonparametric tests against trend. *Econometrica*, **13**, 245–259, https://doi.org/10.2307/1907187.

Meng, X., and Coauthors, 2018: Detecting hydrological consistency between soil moisture and precipitation and changes of soil moisture in summer over the Tibetan Plateau. *Climate Dyn.*, **51**, 4157–4168, https://doi.org/10.1007/s00382-017-3646-5.

Nelson, F. E., and S. I. Outcalt, 1987: A computational method for prediction and regionalization of permafrost. *Arctic and Alpine Research*, **19**, 279–288, https://doi.org/10.2307/1551363.

Oleson, K., and Coauthors, 2013: Technical Description of version 4.5 of the Community Land Model (CLM). NCAR Technical Note, National Center for Atmospheric Research. Available from https://doi.org/10.5065/D6RR1W7M.

Qin, Y. H., and Coauthors, 2016: Using ERA-Interim reanalysis dataset to assess the changes of ground surface freezing and thawing condition on the Qinghai-Tibet Plateau. *Environmental Earth Sciences*, **75**, 826, https://doi.org/10.1007/s12665-016-5633-2.

Slater, A. G., and D. M. Lawrence, 2013: Diagnosing present and future permafrost from climate models. *J. Climate*, **26**, 5608–5623, https://doi.org/10.1175/JCLI-D-12-00341.1.

Swenson, S. C., and D. M. Lawrence, 2012: A new fractional snow-covered area parameterization for the Community Land Model and its effect on the surface energy balance. *J. Geophys. Res.: Atmos.*, **117**, D21107, https://doi.org/10.1029/2012JD018178.

Wu, T. H., L. Zhao, R. Li, Q. X. Wang, C. W. Xie, and Q. Q. Pang, 2013: Recent ground surface warming and its effects on permafrost on the central Qinghai-Tibet Plateau. *International Journal of Climatology*, **33**, 920–930, https://doi.org/10.1002/joc.3479.

Wu, T. H., Y. H. Qin, X. D. Wu, R. Li, D. F. Zou, and C. W. Xie, 2018: Spatiotemporal changes of freezing/thawing indices and their response to recent climate change on the Qinghai-Tibet Plateau from 1980 to 2013. *Theor. Appl. Climatol.*, **132**, 1187–1199, https://doi.org/10.1007/s00704-017-2157-y.

Xie, P. P., and A. Y. Xiong, 2011: A conceptual model for constructing high-resolution gauge-satellite merged precipitation analyses. *J. Geophys. Res.: Atmos.*, **116**, D21106, https://doi.org/10.1029/2011JD016118.

Xie, Z. P., Z. Y. Hu, H. L. Liu, G. H. Sun, Y. X. Yang, Y. Lin, and F. F. Huang, 2017: Evaluation of the surface energy exchange simulations of land surface model CLM4.5 in alpine meadow over the Qinghai-Xizang Plateau. *Plateau Meteorology*, **36**, 1–12, https://doi.org/10.7522/j.issn.1000-0534.2016.00012. (in Chinese with English abstract)

Yao, T. D., and Coauthors, 2012: Different glacier status with atmospheric circulations in Tibetan Plateau and surroundings. *Nature Climate Change*, **2**, 663–667, https://doi.org/10.1038/nclimate1580.

Yin, D. Q., and M. L. Roderick, 2020: A framework to quantify the inter-annual variation in near-surface air temperature due to change in precipitation in snow-free regions. *Environmental Research Letters*, **15**, 114028, https://doi.org/10.1088/1748-9326/abbc94.

Zhang, G. F., Z. T. Nan, L. Zhao, Y. J. Liang, and G. D. Cheng, 2021: Qinghai-Tibet Plateau wetting reduces permafrost thermal responses to climate warming. *Earth and Planetary Science Letters*, **562**, 116858, https://doi.org/10.1016/j.epsl.2021.116858.

Zhao, L., and Coauthors, 2021: A synthesis dataset of permafrost thermal state for the Qinghai-Tibet (Xizang) Plateau, China. *Earth System Science Data*, **13**, 4207–4218, https://doi.org/10.5194/essd-13-4207-2021.

Zhou, C. Y., P. Zhao, and J. M. Chen, 2019: The interdecadal change of summer water vapor over the Tibetan Plateau and associated mechanisms. *J. Climate*, **32**, 4103–4119, https://doi.org/10.1175/JCLI-D-18-0364.1.